IEEE Access
Multidisciplinary ⋮ Rapid Review ⋮ Open Access Journal

Received December 2, 2020, accepted December 13, 2020, date of publication December 21, 2020, date of current version December 31, 2020.

Digital Object Identifier 10.1109/ACCESS.2020.3046300

Insertion of Ag Layer in TiN/SiN_x/TiN RRAM and Its Effect on Filament Formation Modeled by Monte Carlo Simulation

YEON-JOON CHOI[1,2], (Graduate Student Member, IEEE), MIN-HWI KIM[3], SUHYUN BANG[1,2], (Graduate Student Member, IEEE), TAE-HYEON KIM[1,2], (Graduate Student Member, IEEE), DONG KEUN LEE[1,2], (Member, IEEE), KYUNGHO HONG[1,2], (Member, IEEE), CHAE SOO KIM[4], SUNGJUN KIM[5], (Member, IEEE), SEONGJAE CHO[6], (Senior Member, IEEE), AND BYUNG-GOOK PARK[1,2], (Fellow, IEEE)

[1]Inter-University Semiconductor Research Center (ISRC), Seoul National University, Seoul 08826, South Korea
[2]Department of Electrical and Computer Engineering, Seoul National University, Seoul 08826, South Korea
[3]Memory Division, Samsung Electronics, Hwaseong-si 18448, South Korea
[4]Memory Division, Samsung Electronics, Pyeongtaek-si 17786, South Korea
[5]Division of Electronics and Electrical Engineering, Dongguk University, Seoul 04620, South Korea
[6]Department of Electronics Engineering, Gachon University, Seongnam 13120, South Korea

Corresponding author: Byung-Gook Park (bgpark@snu.ac.kr)

This work was supported in part by the National Research Foundation of Korea (NRF) Grant funded by the Korean Government (MSIP) under Grant 2018R1A2A1A05023517, and in part by the Brain Korea 21 Plus Program.

ABSTRACT In this study, the electrical characteristics of TiN/SiN_x/TiN and TiN/Ag/SiN_x/TiN RRAMs were thoroughly investigated through *I-V* measurements. Our novel Ag-inserted silicon nitride-based resistive switching memory (RRAM) achieved switching operation at lower voltages and lower current levels compared to the conventional silicon nitride RRAM that does not have an Ag insertion layer. These enhanced characteristics enable low power operation, one of the main goals of RRAM research. Gradual conductance modulation is also possible in this device with constant voltage pulses being 50% lower than that seen in conventional devices, this property fulfills an important requirement that makes our device suitable for use as a neuromorphic synapse device. The conduction mechanism of our Ag-inserted device was further analyzed through *I-V* measurements and compared with a control group. Based on these data, a 2D Monte Carlo simulation was implemented to investigate the mechanism behind the new behavior displayed by our Ag-inserted silicon nitride RRAM. A resistive network model was used to calculate the voltage and electric field distribution, and then the motion of the particles was simulated by taking into account its relation to the heat generated inside the device.

INDEX TERMS Memristors, Monte Carlo simulation, resistive RAM (RRAM), silver, silicon nitride, synapse device.

I. INTRODUCTION

Resistive switching random access memory (RRAM) is an emerging non-volatile memory (NVM) that stores information by changing the conductance of a switching layer material between top and bottom electrodes. RRAM has drawn a great deal of interest owing to its low power operation, high scalability, and long retention times [1]–[7]. In recent years, a lot of research has been conducted to demonstrate the potential of RRAM as a neuromorphic synapse device [8]–[14]. There have also been some interesting examples of the RRAM's application in chaotic systems and Pavlovian experiments, both of which make excellent use of the variable and dynamic behavior of RRAM [15]–[17]. It has been reported that plenty of electrical insulating materials exhibit resistive switching operation through various mechanisms when an external voltage is applied. Silicon nitride (Si_3N_4) is one of the known RRAM switching layer materials compatible with conventional CMOS fabrication [18]–[25]. In addition, silicon nitride has been used as a hard mask or insulator

The associate editor coordinating the review of this manuscript and approving it for publication was Sun Junwei.

This work is licensed under a Creative Commons Attribution-NonCommercial-NoDerivatives 4.0 License.
For more information, see https://creativecommons.org/licenses/by-nc-nd/4.0/

in CMOS fabrication due to its excellent physical/chemical selectivity and electrical insulating properties. Its role as an electron trapping layer has been widely studied with a view to its use as a charge trap flash (CTF) memory [26]–[28]. Since the resistive switching operation of silicon nitride has been discovered, lots of research has been carried out on the electrical properties of silicon nitride in the context of its use in RRAM [23]–[25], [29]–[32]. Silicon nitride is capable of gradual conductance modulation through a reset operation, this gives it potential for use as a synapse device in neuromorphic systems [33], [34]. However, once a pure silicon nitride RRAM undergoes resistive switching to a low-resistance state, the flowing current level can rise to up to 10^{-2} A and the operating voltage becomes very high for memory applications. These characteristics threaten the low power operation, as such, they do not match one of the main goals of RRAM research. To implement RRAM-based synapses in neuromorphic systems this problem must be tackled. It is reasonable to conclude that we cannot achieve the desired low power memory/neuromorphic characteristics without the help of other materials.

In this work, we took a TiN/SiN_x/TiN stack RRAM and inserted an Ag layer between the top electrode and the switching layer, then we observed any changes in resistive switching characteristics. Silver is known to migrate inside the dielectric under an applied external voltage, RRAM using an active metal is known as conductive-bridging random access memory (CBRAM). In particular, Ag has been studied in synaptic applications because of its similarity to human neurotransmitters found in neurons [35]–[38]. Silicon nitride RRAM using doped silicon as a bottom electrode has been presented before, but many RRAM studies prefer bottom electrodes made out of metal to reduce line resistance in cross-point arrays. We formed the electrode using TiN metal, this is a CMOS fabrication friendly material thanks to it being dry-etchable [39]–[41]. By comparing the differences in performance between our device with an Ag insertion layer and a standard TiN/SiN_x/TiN device as a control group, we were able to identify advances in power consumption and current level controllability. The causes of these enhancements were thoroughly analyzed to clarify the operating mechanism using electrical measurements and observations taken at the microscopic scale. We then implemented a 2D kinetic Monte Carlo simulation that was informed by the measured experimental *I-V* curves to gain a qualitative understanding of the filament formation process in this new RRAM.

II. EXPERIMENT

TiN/Ag/SiN_x/TiN and TiN/SiN_X/TiN RRAMs were fabricated to investigate the role of Ag in the device. The fabrication of the SiN_x switching layer was tried in two thicknesses, 6.5 nm and 11 nm, in order to analyze the conduction mechanism. The thickness of each film was measured by the Nanospec (ST4000-DLX) and the electrical characteristics were measured by the Keithly 4200-SCS semiconductor parameter analyzer and a 4225-RPM pulse signal unit. The material composition of the fabricated device was analyzed by high-resolution transmission electron microscopy (HR-TEM) and an energy dispersive X-ray spectroscopy (EDS) profile was produced using 200 kV accelerating voltage. The silicon oxide was grown on a <100> crystalline silicon wafer by dry oxidation. 100 nm of TiN was deposited by sputtering on the buried oxide, 6.5 nm or 11 nm of SiN_x were then deposited by plasma enhanced CVD (Chemical Vapor Deposition) using 5% SiH_4 (800 sccm), NH_3 (10 sccm), and N_2 (1200 sccm). We tested two groups of RRAM: Ag was not deposited in the control group, and a roughly 40 nm thick Ag layer was deposited in the test group onto the SiN_x film by a thermal evaporator. As the final part of the fabrication process, a TiN capping layer about 100 nm thick was deposited by sputtering. Each RRAM device was patterned to have a 110 μm diameter using a shadow mask.

III. RESULTS AND DISCUSSION

The fabricated RRAM structure is illustrated in Fig. 1(a) and 1(b). The thickness of the deposited 11 nm-SiN_x layer is confirmed in Fig. 1(c) and its x value is calculated to be about 1.10 on average from the EDS profile in Fig. 1(d). The RRAM stores information by switching between HRS (High Resistance State) and LRS (Low Resistance State) according to an external voltage signal, its electrical characteristics are presented in Fig. 2. Fig. 2(a) and 2(b) show DC sweep *I-V* characteristics of the RRAM devices with and without an Ag insertion layer on top of the SiN_x layer, respectively. The thickness of the SiN_x layer is 6.5 nm and 11 nm for Fig. 2(a) and 2(b) respectively. Both RRAM devices with and without an Ag insertion layer over an 11 nm SiN_x layer show non-volatile memory operation with bipolar resistive switching characteristics after the forming operation. The TiN/11 nm-SiN_x/TiN RRAM has a forming voltage around 8 V or 7.2 MV/cm, which nearly corresponds to the dielectric strength of the silicon nitride deposited by plasma enhanced CVD [42]. After the forming process, the set/reset switching operations are performed with an On/Off switching ratio of nearly 100, this is sufficient for normal memory applications. However, the operating current level of the TiN/11 nm-SiN_x/TiN device far exceeds its I_{cc} (compliance current) of 10^{-6} A, showing high current overshoot in the SiN_x resistive switching layer. On the contrary, the Ag insertion layer causes significant changes in the switching characteristics of the TiN/SiN_x/TiN device. The forming, set, and reset voltages of the TiN/Ag/11 nm-SiN_x/TiN RRAM are significantly lowered with an Ag insertion layer between the capping layer and the switching layer. The switching voltages of the TiN/Ag/11 nm-SiN_x/TiN RRAM device are statistically shown in Fig. 2(c), these results indicate that the Ag insertion layer plays a role in reducing the operating voltage by more than 50% compared to the RRAM device without an Ag insertion layer. Furthermore, the LRS of the TiN/Ag/SiN_x/TiN RRAM device is able to return to a HRS that is similar to its pristine resistance level after the reset process, this shows the potential of flexible conductive

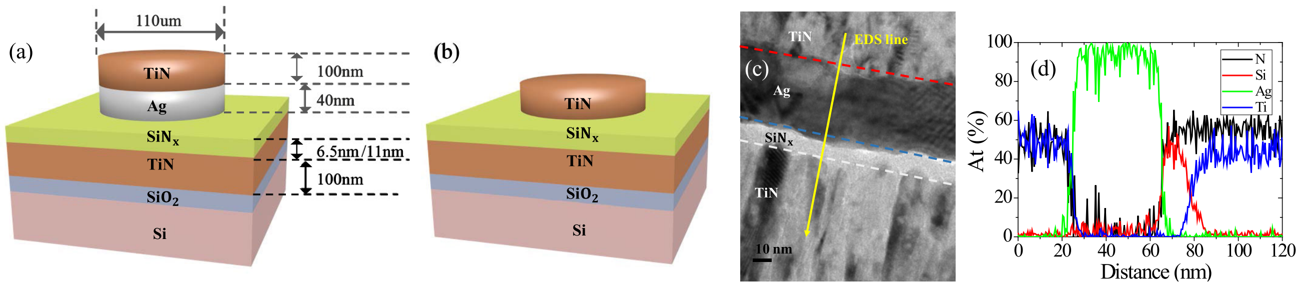

FIGURE 1. Fabricated RRAM single cell (a) with an Ag insertion layer and (b) the control without Ag layer. Figure (c) and (d) are the transmission electron microscopy (TEM) image and the EDS profile, respectively, for the TiN/Ag/11 nm-SiN_X/TiN RRAM. The x value of the off-stoichiometric SiN_X film is 1.10 on average, showing a silicon rich nitride.

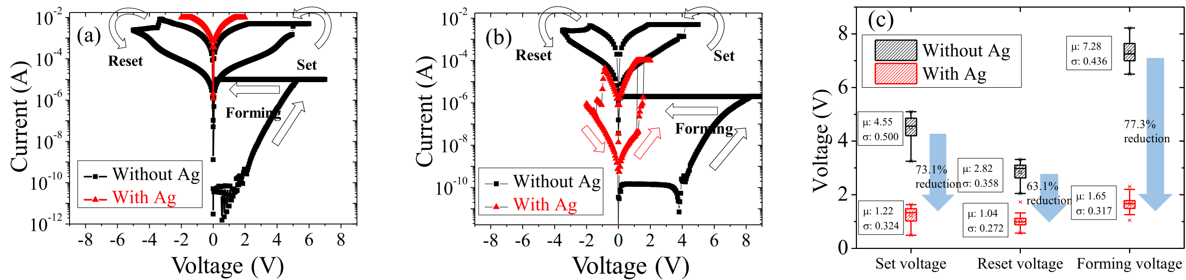

FIGURE 2. DC sweep IV curves of (a) a 6.5 nm SiN_X and (b) a 11 nm SiN_X RRAM devices. (c) The operating voltage statistics of 11 nm SiN_X RRAM. The reset voltage is defined as the point at which conductance begins to decrease.

filaments in this device. Meanwhile, the devices in this stack show higher operating voltages and LRS/HRS resistances compared to the usual, commonly investigated Ag based RRAMs that tend to operate below 1V [35], [43]–[47]. The operating voltage varies greatly depending on the type and thickness of the insulator [43], [44]. As such, although two types of RRAM may contain some of the same material, different structures or physical dimensions can lead to quite different measured characteristics without contradiction. The cause behind this sensitivity to the type and thickness of the insulator is not clear and further research on silicon nitride as a path for Ag ions is required. However, these higher operating voltages and LRS/HRS resistances are actually rather desirable from the perspective of neuromorphic systems. Spiking neural networks, a leading learning approach in neuromorphic systems, are introducing integrate & fire circuits to mimic biological neurons [48]. The value of the spiking voltage is determined by the threshold voltage of the MOSFETs in the inverter and this value is at least 1V [48]. Therefore, any RRAMs with an operating voltage lower than 1V are not suitable for use as synapses in such systems because they are susceptible to their synaptic weights being changed even during the inference step.

Fig. 3 shows the split of resistance levels according to various I_{cc}s in the 11 nm SiN_x RRAM devices with or without an Ag insertion layer. In general, RRAM devices do not show self-compliance, therefore, adding a selector material layer or connecting a transistor to the device is required to limit the current flow in the RRAM [49]–[51]. In this case, the measurement equipment (4200-SCS) sets the I_{cc} to limit the current flow. The TiN/Ag/SiN_x/TiN RRAM can be adjusted to several resistance states using current compliance whereas the device without an Ag insertion layer cannot do this. The *I-V* curve corresponding to I_{cc} of 10^{-6} A shows an abrupt set behavior in the forward bias sweep, but the LRS is hidden during the reset process in the reverse bias sweep, which is a volatile memory operation. The conductive filament, probably related to the Ag insertion layer, has ruptured by the end of the forward bias sweep. A study on the electrical factors that determine the volatility of the memory will be performed in a later study, but it is clear that the Ag insertion layer has the effect of reducing the current overshoot and makes it possible to control the strength of the conductive filament formed in the SiN_x switching layer. The retention data of the RRAM with the Ag insertion layer in Fig. 3(c) supports this idea since the volatility of the LRS decreases with increasing I_{cc}. The presence of Ag layer is expected to prevent sudden changes in conductance even during voltage pulse operation. Fig. 4 compares the gradual set/reset operation under a voltage pulse train in the TiN/11 nm-SiN_X/TiN RRAM devices with and without an Ag insertion layer. The devices are initially set to a HRS where a conductive path has already been formed once. Fig. 4(a) shows their reaction to a set and reset pulse scheme with a read voltage of 0.1 V. The RRAM device with an Ag insertion layer exhibits a nearly 500% range of conductance at a lower programming voltage of 1.5 V, this is in contrast to the programming voltage of the device without an Ag insertion layer. The reproduction of the continuous gradual switching in TiN/Ag/SiN_x/TiN RRAM is statistically shown in Fig. 4(c). Also, the much lower conductance level during pulse operation makes it efficient in terms of power consumption. Gradual resistive

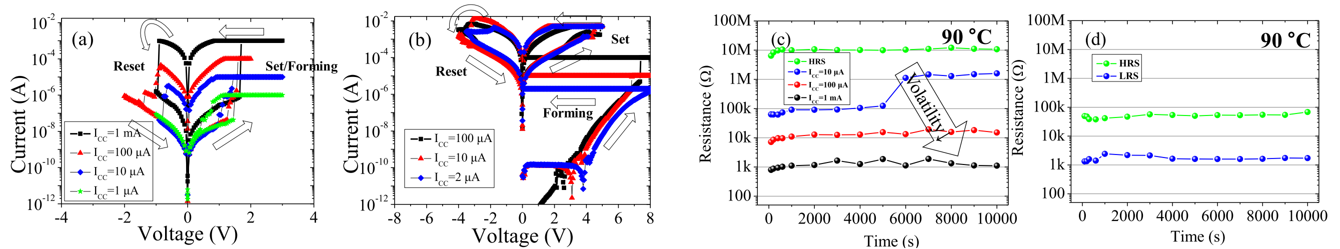

FIGURE 3. Compliance current controlled *I-V* characteristics in 11 nm SiN_X RRAM devices (a) with and (b) without Ag layer. The retention data of the (c) TiN/Ag/11 nm-SiN_X/TiN shows the I_{CC}-controlled non-volatile operation and also shows a wider range of expressible conductance compared to the retention data of the (d) TiN/11 nm-SiN_X/TiN RRAM.

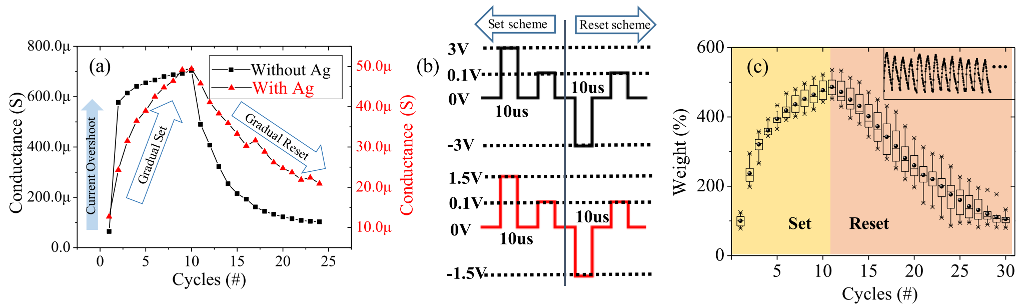

FIGURE 4. Non-volatile gradual switching characteristics of 11 nm-SiN_X RRAM (a) with and without an Ag insertion layer and (b) the corresponding voltage pulse scheme. (c) The continuous gradual switching characteristics of the RRAM with an Ag insertion layer are statistically shown.

switching characteristics in both set and reset processes are advantageous for fine conductance tuning and are essential for neuromorphic application where RRAM is used as a synapse device [52]–[54]. The pure silicon nitride RRAM also exhibits a gradual reset operation, but due to its relatively low linearity, it is difficult to expect high recognition rates in a spiking neural network. In addition, RRAM with an Ag insertion layer shows gradual resistive switching without the Increasing Step Pulse Program (ISPP) scheme, that is optimized for application to simple neuron circuits where constant spiking voltages are produced as an output [55]–[58]. The low programming voltage and conductance of the RRAM with an Ag insertion layer result in more than 90% power efficiency for the gradual set/reset process as shown in Fig. 5(a) and 5(b).

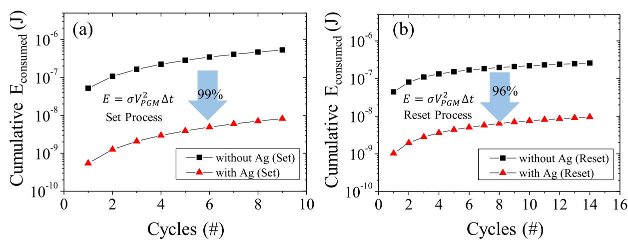

FIGURE 5. Cumulative energy consumed during (a) set and (b) reset process. σ denotes the conductance and σV_{PGM} represents the current.

The reduction in the operating voltage of RRAM is due to some sort of new switching mechanism that differs from that in pure silicon nitride. Ag has been reported to form Ag clusters inside dielectric materials when deposited and can extend in the direction of the electric field [35], [38]. The TiN/Ag/SiN_x/TiN RRAM shows several signs of Ag clusters being formed in the thin SiN_x film. Evidence of these Ag clusters is shown in the TEM images of Fig. 6(a) and 6(b). Some Ag can be seen to penetrate into the interface between the Ag and 11 nm-SiN_x layers, resulting in an uneven Ag layer surface. Some Ag became separated from the Ag layer surface and formed clusters with a size of 2 to 6 nm. Assuming the internal diagram of the 11 nm SiN_x switching layer as shown in Fig. 6(c), the conduction mechanism can be explained by Fig. 6(d) and 6(e). The silicon nitride follows P-F (Poole-Frenkel) conduction where a leakage current is generated by electrons hopping between conduction level traps as mentioned in previous studies [59]–[61]. The Ag clusters dissolved in the SiN_x shorten the effective hopping distance, making it closer to ohmic conduction through the Ag material. This tendency is more evident in a thinner film as the Ag clusters occupy a higher proportion of the space between electrodes as indicated in Fig. 2(a). The pristine TiN/Ag/6.5 nm-SiN_x/TiN RRAM device shows short-circuited resistance despite the absence of a forming process whereas the pristine TiN/6.5 nm-SiN_x/TiN RRAM device just shows higher leakage current compared to TiN/11 nm-SiN_x/TiN RRAM due to a thinner SiN_x layer. Fig. 7 describes our hypothesis for how Ag contributes to the conduction mechanism. The conduction mechanism of the pristine TiN/SiN_x/TiN RRAM is analyzed by fitting its *I-V* measurement data using both P-F conduction and Ohmic conduction plots in Fig. 7(a). Although both P-F and Ohmic plots show a linear curve, the slope of the line in the Ohmic plot far exceeds 1, proving that the leakage current

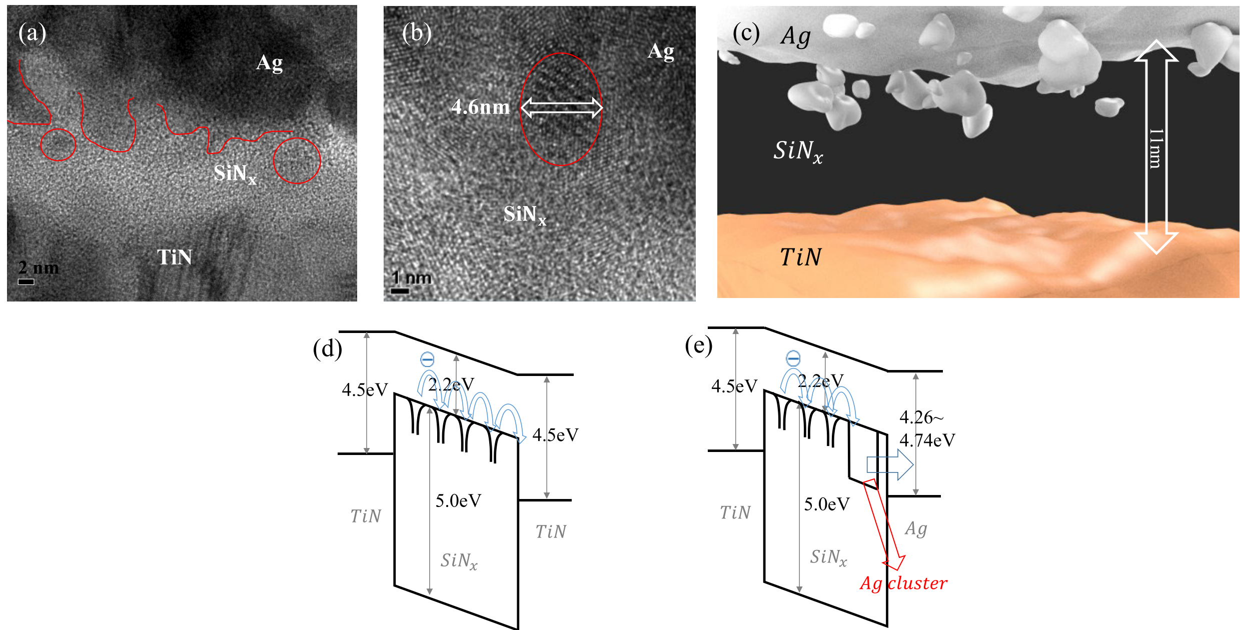

FIGURE 6. (a), (b) TEM images of silver clusters that are dissolved in the 11 nm-SiN_x interface, resulting in higher leakage in the pristine RRAM and (c) a plausible 3D-diagram of the RRAM device. The energy band diagram is compared between SiN_x switching layers (d) without and (e) with an Ag insertion layer to understand the conduction mechanism.

in the pure SiN_x follows P-F conduction. In Fig. 7(b), both RRAM devices with and without an Ag insertion layer show clear Ohmic conduction in LRS, and space charge limited current (SCLC) conduction in HRS. However, the SCLC conduction of the TiN/SiN_x/TiN RRAM device in HRS has a steep rising region around 4 V whereas the TiN/Ag/SiN_x/TiN RRAM in HRS does not. The rising part in the SCLC region is related to the trap filled limited current that occurs when the conduction is influenced by a large number of traps in the insulator [62], [63]. This shows that a trap-related conduction mechanism is predominant in the pure SiN_x whereas this is masked in Ag-containing insulator, indicating that conducting filaments in TiN/SiN_x/TiN and TiN/Ag/SiN_x/TiN RRAMs are mainly composed of pure silicon nitride traps and Ag atoms, respectively, as illustrated in Fig. 7(c) and 7(d). Ag is known to be ionized and to migrate interstitially along the direction of the electric field distributed in dielectrics [35], [38]. If so, the initial forming voltage of the TiN/Ag/SiN_x/TiN device will differ depending on the direction of the voltage applied to the anode and cathode due to the asymmetric structure. In Fig. 8(a), the forming voltage of the TiN/Ag/11 nm-SiN_x/TiN under reverse bias is obviously higher than that under forward bias operation and the statistical distributions of forward and reverse forming voltages are shown in Fig. 8(b). The increase of the forming voltage during the reverse bias sweep implies that the effect of Ag on filament formation is reduced and the high dielectric breakdown characteristics of SiN_x are revealed, like is seen in the illustration Fig. 8(c). From the above analysis, it can be inferred that the filament formed under the forward bias sweep is obviously due to the movement of Ag atoms rather than due to trap generation. In addition, the Ag atoms tend to move in the direction from the positive towards the negative potential as depicted in Fig. 8(d). From the analysis so far, it is clear that the various changes observed in the SiNx RRAM switching operation are derived from the Ag insertion layer. The principle of the operation of our TiN/Ag/SiN_x/TiN RRAM does not seem to differ from other general redox memories, however, the presence of the Ag clusters and traps due to the use of off-stoichiometric silicon nitride as an insulator gives rise to a difference between the mechanism we propose and that proposed in previous works.

IV. MONTE CARLO SIMULATION

It is important to understand the filament formation and its corresponding *I-V* curves in order to improve the performance of the RRAM. The following simulation shows how the Ag atoms move inside the device and how they influence the formation of conducting filament inside the insulator. We here make three assumptions: (i) there is a certain probability Ag will be ionized and migrate along the direction of the internal electric field distribution. Conventional electro-chemical studies on CBRAM have shown that the oxidation of active metals such as Ag, Cu, Ni and Co occurs given sufficient amount of positive voltage [37], [64]–[67]. (ii) The current flows by Ohmic conduction, but the conduction amount varies exponentially with the distance from Ag atoms due to the tunneling effect. (iii) Ionized Ag cations are more likely to be reduced back to metal atoms when they touch the cathode or virtual Ag ground. Assumptions (ii) and (iii) can be scarcely found in previous studies and help make our simulation and analysis unique. Several calculations and graph extractions were performed with Python 3.6.3. The mesh was implemented as a rectangular shape using the FDM

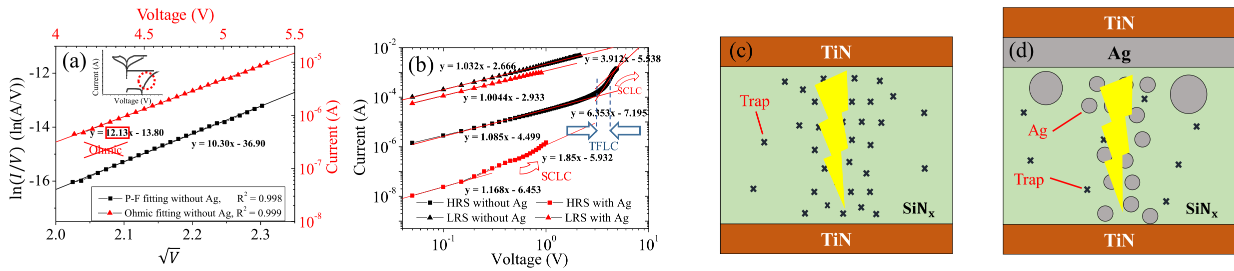

FIGURE 7. (a) A P-F/SCLC fitting graph of a pristine TiN/11 nm-SiN_x/TiN RRAM, and (b) a SCLC fitting graph of both RRAM devices with and without an Ag insertion layer. Traps and Ag atoms distributed in (c) TiN/SiN_x/TiN and (d) TiN/Ag/SiN_x/TiN RRAM devices after filament forming process. Each of them mainly contributes to the electrical conduction of the RRAM device.

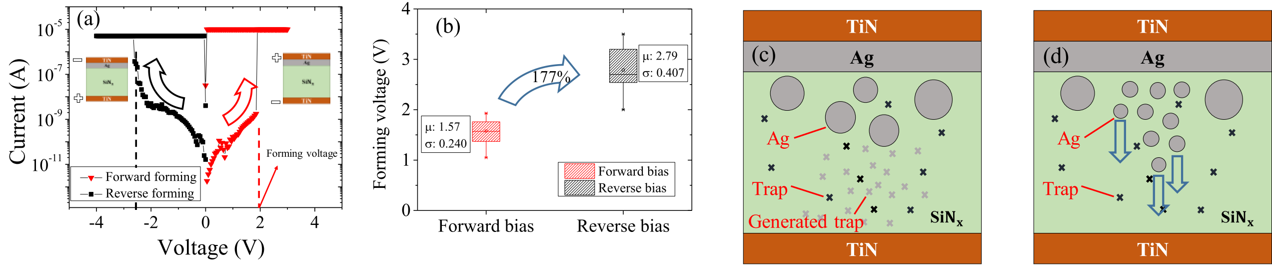

FIGURE 8. (a) The *I-V* curves of the TiN/Ag/11 nm-SiN_x/TiN RRAM device depending on the initial forming bias direction, and (b) the statistics on the forming voltage. The expected switching model depending on (c) the reverse bias and (d) the forward bias forming processes.

(Finite Difference Method) and the vertices of the meshes generated in the RRAM represents the location of each SiN_x molecule. The distance a between the vertices was determined to be 0.419 nm, which corresponds to the intrinsic density of Si_3N_4, this was derived from:

$$a = \left(\sqrt[3]{\frac{\rho}{M} N_A}\right)^{-1} \tag{1}$$

where ρ, M, N_A denote the density, molecular weight, and Avogadro constant of the SiN_x. The physical and chemical transitions of all molecules or atoms in the switching layer occur according to the rules of simple Transition State Theory (TST) with a rate of [68]:

$$\Gamma = \upsilon \exp\left(-\frac{E_a - \Delta V}{k_b T}\right) \tag{2}$$

for a two-dimensional area, where υ, k_b, T denote the lattice vibration frequency, Boltzmann constant, and temperature [69]–[72]. ΔV is the chemical potential difference between two neighboring vertices in a mesh. Instead of the Poisson equation, a new resistance network system is introduced to obtain the chemical voltage distribution inside the switching layer using Kirchhoff's equation:

$$V_{point} = (R_{left} || R_{right} || R_{up} || R_{down}) \sum_{i=1}^{4} \frac{V_i}{R_i} \tag{3}$$

as depicted in Fig. 9(a). The activation energies for migrations and chemical reactions in (2) are modeled in the Monte Carlo simulation as shown in Fig. 9(b). A decrease in resistance due to the tunneling transmission coefficient between metal atoms was applied in order to simulate the increase in RRAM conductance that occurs even when Ag atoms are not completely connected to each other as a conducting bridge.

$$\Delta\sigma' = \sigma_0 \exp\left(-\frac{2L}{\hbar}\sqrt{2m_{eff}\,\Delta E_{fermi}}\right) \tag{4}$$

L, m_{eff}, ΔE_{fermi} denote the distance from a metal atom, effective electron mass in Si_3N_4, and the conduction level difference between Ag and Si_3N_4. $Ea_{1,2}$ are energies related to the emission and desorption of Ag atoms at the boundary of the Ag redundant source. The emitted Ag cations migrate through the SiN_x switching layer with Ea_9 activation energy. The Ag cations tend to be reduced to metal atoms with $Ea_{3\sim5}$ activation energies when adjacent to the bottom electrode, and ionized back to the cations with $Ea_{6\sim8}$ activation energies. Each of the three activation energies is defined by the number of surrounding Ag atoms. The calculated current distribution from the resistor network scheme induces power to be generated at each vertex of the mesh, then the heat distribution inside the RRAM is calculated using (5), which is also known as the heat transfer equation.

$$c\rho\frac{\partial T}{\partial t} = k\nabla^2 T + \frac{I^2 R \Delta t}{dV} (= Q_H) \tag{5}$$

c, ρ, T, k, dV, I R, Δt denote the specific heat capacity, density, temperature, thermal conductivity, minimal volume, current, resistance, and minimal time step in the simulation. Δt is defined by the speed of the DC sweep given in the simulation. The heat term Q_H represents the internal heat generated by joule heating, its dimension is J/m^3. The explicit FDM method cannot ensure stable and fast calculations over time when the distance between vertices is extremely small [73], [74]. Therefore, the implicit FDM method was used to solve the second order partial differential equations without

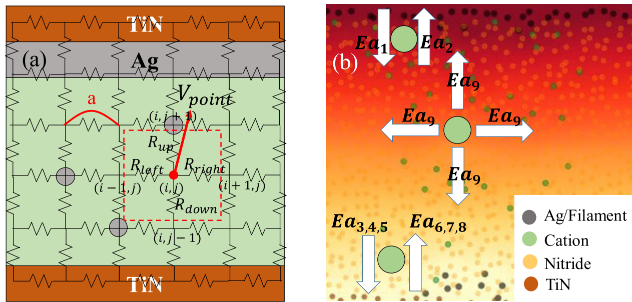

FIGURE 9. (a) A resistor network scheme for calculation of chemical potential. (b) The definition of physical and chemical transition activation energies for Ag atoms.

divergence of the solution over time. The specific heat capacity, resistivity, density, and molecular weight are all applied according to the intrinsic values of Ag, Si_3N_4 and TiN, the simulation parameters are summarized in Table 1 and 2. A DC sweep Monte Carlo simulation was conducted according to the flowchart depicted in Fig. 10.

TABLE 1. Material parameters used in the simulation.

	c (J/kg·K)	ρ (kg/m^3)	k (W/m·K)	σ_0(S/m)
Ag	2.40×10^2	1.049×10^4	429	6.58×10^7
SiN_x	8.00×10^2	3.170×10^3	40	$\sim10^{-14}$
TiN	3.88×10^2	5.210×10^3	29	2.5×10^5

TABLE 2. Simulation parameters.

Parameters	Value	Parameters	Value
Ea_1	0.69 eV	υ	10^{14} Hz
Ea_2	0.7 eV	a	0.419 nm
Ea_3	0.7 eV	m_{eff}	$0.5m_e$ [75], [76]
Ea_4	0.6 eV	m_e	9.11×10^{-31} kg
Ea_5	0.5 eV	k_b	1.38×10^{-23} J/K
Ea_6	0.7 eV	$\hbar$	1.05×10^{-34} J·s
Ea_7	0.8 eV	Δt	10^{-3} s
Ea_8	0.9 eV		
Ea_9	0.4 eV		

Several silver clusters were placed near the top electrode at the initial simulation step as shown in Fig. 11. It was confirmed that these silver clusters were ionized and migrates to the bottom electrode, serving as the foundation for a filament to grow. The Monte Carlo simulation results of conductive filament formation process with different compliance currents (10^{-7} A, 10^{-6} A, 10^{-5} A, and 10^{-4} A) are depicted in Fig. 12(a)-(d). The filaments are generally formed in the 1.5∼1.7 V range of external voltage, and the corresponding Ag oxidation activation energy applied in this simulation is 0.69 eV as shown in Table 2. This value is similar to the difference between the work function and the absolute oxidation potential (WF-AOP) of silver, i.e., 0.62 eV [67], which is the energy barrier for the oxidation. As an external voltage is applied, the silver cations that are ionized from

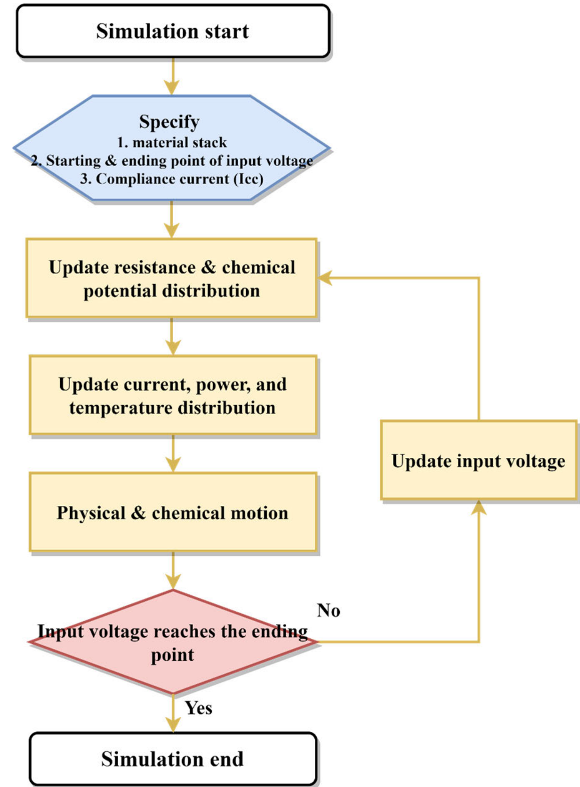

FIGURE 10. Flowchart for DC sweep in Monte Carlo simulation.

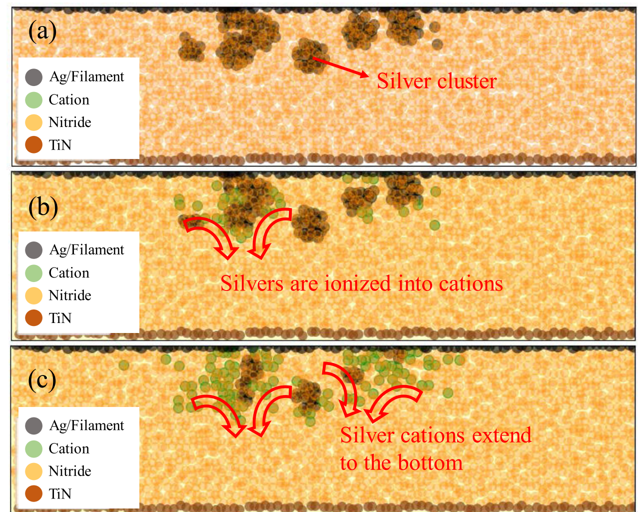

FIGURE 11. (a) The silver clusters are placed near the top electrode in the initial step of the Monte Carlo simulation. As the voltage increases, (b) the silver clusters and the silver atoms in the top electrode are ionized into cations and (c) extend to the bottom electrode to form a foundation for a filament to grow.

the silver clusters and the top electrode gain electrons at the bottom electrode and are reduced to a local virtual ground. This virtual ground acts as a lightning rod, forming a localized filament which prevents the extensive and powerful breakdown of the silicon nitride. In addition, the lateral effective thickness of the conductive filament becomes controllable with compliance currents, this explains the effect of the

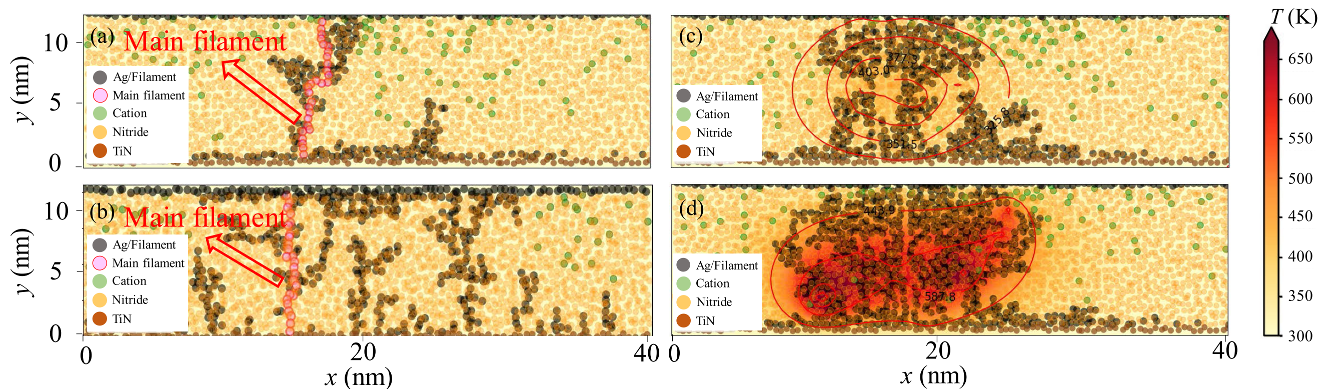

FIGURE 12. Monte Carlo simulation results for conductive filament formation process in TiN/Ag/11 nm-SiN_x/TiN RRAM according to compliance currents of (a) 10^{-7} A, (b) 10^{-6}A, (c) 10^{-5}A, and (d) 10^{-4}A. A filament is composed of Ag atoms that were supplied from the silver clusters and the top electrode.

current overshoot reduction seen in Fig. 3. The controllable effective filament thickness without further current overshoot is important as it leads to the gradual set/reset operations capability. In the cases where the compliance current is set below 10^{-6} A, the current path is formed that is thin enough to specify the main current path within the filament. The current is concentrated in this main current path, making the filament vulnerable to spontaneous disruption like a volatile memory operation as shown in Fig. 3(a). The background color indicates the kelvin temperature generated by joule heating, which is calculated from (5). The higher compliance current over 10^{-6} A allows the flowing current to generate more heat in the switching layer and increase the internal temperature. The increased temperature consequently accelerates the supply of Ag atoms from the top electrode. These supplied Ag atoms fiercely vibrate due to the elevated heat, and the atoms try to migrate and occupy spaces between each other, leading them to settle into a thick filament. As the conductive filament thickens, the concentrated current is dispersed through the widened filament and the internal heat finds a convergence point. This thickened filament formed through the preceding series of processes is no longer susceptible to external stimuli, and a non-volatile operation takes place. Since this simulation is constrained to 2-dimensions, its use for fully quantitative analysis is limited. Nevertheless, this approach works nicely as a qualitative analysis since it is sufficient to demonstrate the trends shown in electrical measurements and gives corresponding filament shapes that are quite reasonable.

V. CONCLUSION

The effect of an Ag insertion layer on the electrical characteristics of TiN/SiN_x/TiN RRAM was investigated using *I-V* measurements. The Ag layer was found to significantly lower the operating voltage and current of the device while suppressing current overshoot. This device shows great potential for use as a neuromorphic synapse due to its gradual switching operation. The conduction and switching mechanism was closely analyzed and a Monte Carlo simulation was conducted. Through this we were able to understand the filament formation process occurring in the TiN/Ag/SiN_x/TiN RRAM and how it relates to the compliance current and *I-V* measurement results. This work is expected to provide some guidance for follow-up RRAM studies pursuing the fabrication of the kind of devices that can achieve low power operation through the use of an Ag insertion layer.

REFERENCES

[1] A. Chen, "A review of emerging non-volatile memory (NVM) technologies and applications," *Solid-State Electron.*, vol. 125, pp. 25–38, Nov. 2016.

[2] Y. Chen, "ReRAM: History, status, and future," *IEEE Trans. Electron Devices*, vol. 67, no. 4, pp. 1420–1433, Apr. 2020.

[3] S. Munjal and N. Khare, "Advances in resistive switching based memory devices," *J. Phys. D, Appl. Phys.*, vol. 52, no. 43, Aug. 2019, Art. no. 433002.

[4] J. J. Yang, D. B. Strukov, and D. R. Stewart, "Memristive devices for computing," *Nature Nanotechnol.*, vol. 8, no. 13, pp. 13–24, Dec. 2012.

[5] U. Das, S. Bhattacharjee, P. K. Sarkar, and A. Roy, "A multi-level bipolar memristive device based on visible light sensing MoS_2 thin film," *Mater. Res. Exp.*, vol. 6, no. 7, Apr. 2019, Art. no. 075037.

[6] S. K. Vishwanath and J. Kim, "Resistive switching characteristics of all-solution-based Ag/TiO_2/Mo-doped In_2O_3 devices for non-volatile memory applications," *J. Mater. Chem. C*, vol. 4, no. 46, pp. 10967–10972, Oct. 2016.

[7] R. Zazpe, M. Ungureanu, F. Golmar, P. Stoliar, R. Llopis, F. Casanova, D. F. Pickup, C. Rogero, and L. E. Hueso, "Resistive switching dependence on atomic layer deposition parameters in HfO_2-based memory devices," *J. Mater. Chem. C*, vol. 2, no. 17, pp. 3204–3211, Nov. 2014.

[8] X. Hong, D. J. Loy, P. A. Dananjaya, F. Tan, C. Ng, and W. Lew, "Oxide-based RRAM materials for neuromorphic computing," *J. Mater. Sci.*, vol. 53, no. 12, pp. 8720–8746, Feb. 2018.

[9] Z. Wang, M. Yin, T. Zhang, Y. Cai, Y. Wang, Y. Yang, and R. Huang, "Engineering incremental resistive switching in TaO_x based memristors for brain-inspired computing," *Nanoscales*, vol. 8, no. 29, pp. 14015–14022, Apr. 2016.

[10] T. Dalgaty, M. Payvand, F. Moro, D. R. B. Ly, F. Pebay-Peyroula, J. Casas, G. Indiveri, and E. Vianello, "Hybrid neuromorphic circuits expoiting non-conventional properties of RRAM for massively parallel local plasticity mechanisms," *APL Mater.*, vol. 7, no. 8, Aug. 2019, Art. no. 081125.

[11] K. Moon, S. Lim, J. Park, C. Sung, S. Oh, J. Woo, J. Lee, and H. Hwang, "RRAM-based synapse devices for neuromorphic systems," *Faraday Discuss.*, vol. 213, pp. 421–451, Feb. 2019.

[12] Y. Matveyev, K. Egorov, A. Markeev, and A. Zenkevich, "Resistive switching and synaptic properties of fully atomic layer deposition grown TiN/HfO_2/TiN devices," *J. Appl. Phys.*, vol. 117, no. 4, Jan. 2015, Art. no. 044901.

[13] V. Milo, C. Zambelli, P. Olivo, E. Perez, M. K. Mahadevaiah, O. G. Ossorio, C. Wenger, and D. lemini, "Multilevel HfO_2-based RRAM devices for low-power neuromorphic networks," *APL Mater.*, vol. 7, no. 8, Aug. 2019, Art. no. 081120.

[14] T. Ohno, T. Hasegawa, T. Tsuruoka, K. Terabe, J. K. Gimzewski, and M. Aono, "Short-term plasticity and long-term potentiation mimicked in single inorganic synapses," *Nature Mater.*, vol. 10, pp. 591–595, Aug. 2011.

[15] J. Sun, X. Zhao, J. Fang, and Y. Wang, "Autonomous memristor chaotic systems of infinite chaotic attractors and circuitry realization," *Nonlinear Dyn.*, vol. 94, no. 4, pp. 2879–2887, Aug. 2018.

[16] Y. Yu, H. Ma, C. Yang, N. Yang, Y. Wang, X. Wang, T. Nyima, and M. Wang, "Chaotic circuit based on memristive elements," in *Proc. IEEE Conf. Ind. Electron. Appl. (ICIEA)*, Xi'an, China, Jun. 2019, pp. 1112–1116.

[17] J. Sun, G. Han, Z. Zeng, and Y. Wang, "Memristor-based neural network circuit of full-function pavlov associative memory with time delay and variable learning rate," *IEEE Trans. Cybern.*, vol. 50, no. 7, pp. 2935–2945, Jul. 2020.

[18] X. Chen, W. Hu, Y. Li, S. Wu, and D. Bao, "Complementary resistive switching behaviors evolved from bipolar TiN/HfO_2/Pt device," *Appl. Phys. Lett.*, vol. 108, no. 5, Jan. 2016, Art. no. 053504.

[19] H. Jiang and D. A. Stewart, "Enhanced oxygen vacancy diffusion in Ta_2O_5 resistive memory devices due to infinitely adaptive crystal structure," *J. Appl. Phys.*, vol. 119, no. 13, Mar. 2016, Art. no. 134502.

[20] L. Ji, Y.-F. Chang, B. Fowler, Y.-C. Chen, T.-M. Tsai, K.-C. Chang, M.-C. Chen, T.-C. Chang, S. M. Sze, E. T. Yu, and J. C. Lee, "Integrated one diode–one resistor architecture in nanopillar SiO_x resistive switching memory by nanosphere lithography," *Nano Lett.*, vol. 14, no. 2, pp. 813–818, Dec. 2013.

[21] Z.-H. Tan, R. Yang, K. Terabe, X.-B. Yin, and X. Guo, "Revival of 'dead' memristive devices: Case of WO_{3-x}," *Phys. Chem. Chem. Phys.*, vol. 18, no. 3, pp. 1392–1396, Dec. 2015.

[22] X. Jiang, Z. Ma, H. Yang, J. Yu, W. Wang, W. Zhang, W. Li, J. Xu, L. Xu, K. Chen, X. Huang, and D. Feng, "Nanocrystalline Si pathway induced unipolar resistive switching behaviour from annealed Si-rich SiN_x/SiN_y multilayers," *J. Appl. Phys.*, vol. 116, no. 12, Sep. 2014, Art. no. 123705.

[23] S. Kim, S. Jung, M.-H. Kim, T.-H. Kim, S. Bang, S. Cho, and B.-G. Park, "Nano-cone resistive memory for ultralow power operation," *Nanotechnol.*, vol. 28, no. 12, Feb. 2017, Art. no. 124207.

[24] S. Kim, S. Cho, and B.-G. Park, "Fully Si compatible SiN resistive switching memory with large self-rectification ratio," *AIP Adv.*, vol. 6, no. 1, Jan. 2016, Art. no. 015021.

[25] S. Kim, S. Jung, M.-H. Kim, S. Cho, and B.-G. Park, "Resistive switching characteristics of Si_3N_4-based resistive-switching random-access memory cell with tunnel barrier for high density integration and low-power applications," *Appl. Phys. Lett.*, vol. 106, no. 21, May 2015, Art. no. 212106.

[26] S. Choi, H. Yang, M. Chang, S. Baek, H. Hwang, S. Jeon, J. Kim, and C. Kim, "Memory characteristics of silicon nitride with silicon nanocrystals as a charge trapping layer of non-volatile memory devices," *Appl. Phys. Lett.*, vol. 86, no. 25, Jun. 2005, Art. no. 251901.

[27] M.-H. Jung, K. S. Kim, G. H. Park, and W. J. Choi, "Dependence of charge trapping and tunneling on the silicon-nitride (Si_3N_4) thickness for tunnel barrier engineered non-volatile memory applications," *Appl. Phys. Lett.*, vol. 94, no. 5, Feb. 2009, Art. no. 053508.

[28] E. Vianello, F. Driussi, P. Blaise, P. Palestri, D. Esseni, L. Perniola, G. Molas, B. D. Salvo, and L. Selmi, "Explanation of the charge trapping properties of silicon nitride storage layers for NVMs-Part II: Atomistic and electrical modelling," *IEEE Trans. Electron Devices*, vol. 58, no. 8, pp. 2490–2499, Jun. 2011.

[29] S. Kim and B.-G. Park, "Nonlinear and multilevel resistive switching memory in Ni/Si_3N_4/Al_2O_3/TiN structures," *Appl. Phys. Lett.*, vol. 108, no. 21, May 2016, Art. no. 212103.

[30] H.-D. Kim, M. Yun, and S. Kim, "Self-rectifying resistive switching behaviour observed in Si_3N_4-based resistive random access memory devices," *J. Alloys Compounds*, vol. 651, pp. 340–343, Dec. 2015.

[31] J. Y. Kwon, J. H. Park, and T. G. Kim, "Self-rectifying resistive-switching characteristics with ultralow operating currents in SiO_xN_y/AlN bilayer devices," *Appl. Phys. Lett.*, vol. 106, no. 22, Jun. 2015, Art. no. 223506.

[32] X. Jiang, Z. Ma, J. Xu, K. Chen, L. Xu, W. Li, X. Huang, and D. Feng, "A-SiN_x: H-based ultra-low power resistive random access memory with tunable Si dangling bond conduction paths," *Sci. Rep.*, vol. 5, Oct. 2015, Art. no. 15762.

[33] S. Kim and B.-G. Park, "Improved multi-level capability in Si_3N_4-based resistive switching memory using continuous gradual reset switching," *J. Phys. D, Appl. Phys.*, vol. 50, no. 2, Nov. 2016, Art. no. 02LT01.

[34] S. Kim, S. Jung, M.-H. Kim, S. Cho, and B.-G. Park, "Gradual bipolar resistive switching in Ni/Si_3N_4/n^+-Si resistive-switching memory device for high-density integration and low-power applications," *Solid-State Electron.*, vol. 114, pp. 94–97, Dec. 2015.

[35] Z. Wang, S. Joshi, S. E. Savel'ev, H. Jiang, R. Midya, P. Lin, M. Hu, N. Ge, J. P. Strachan, Z. Li, Q. Wu, M. Barnell, G.-L. Li, H. L. Xin, R. S. Williams, Q. Xia, and J. J. Yang, "Memristors with diffusive dynamics as synaptic emulators for neuromorphic computing," *Nature Mater.*, vol. 16, pp. 101–108, Sep. 2016.

[36] S. H. Jo, T. Chang, I. Ebong, B. B. Bhadviya, P. Mazumder, and W. Lu, "Nanoscale memristor device as synapse in neuromorphic systems," *Nano Lett.*, vol. 10, no. 4, pp. 1297–1301, Mar. 2010.

[37] Q. Liu, J. Sun, H. Lv, S. Long, K. Yin, N. Wan, Y. Li, L. Sun, and M. Liu, "Real-time observation on dynamic growth/dissolution of conductive filaments in oxide-electrolyte based ReRAM," *Adv. Mater.*, vol. 24, no. 14, pp. 1844–1849, Mar. 2012.

[38] S. Li, F. Zeng, C. Chen, H. Liu, G. Tang, S. Gao, C. Song, Y. Lin, F. Pan, and D. Guo, "Synaptic plasticity and learning behaviours mimicked through Ag interface movement in an Ag/conducting polymer/Ta memristive system," *J. Mater. Chem. C*, vol. 1, no. 34, pp. 5292–5298, Jun. 2013.

[39] F. Fracassi, R. d'Agostino, R. Lamendola, and I. Mangieri, "Dry etching of titamium nitride thin films in CF_4-O_2 plasmas," *J. Vac. Sci. Technol. A, Vac. Surf. Films*, vol. 13, no. 2, pp. 335–342, Jun. 1998.

[40] S. R. Min, H. N. Cho, Y. L. Li, S. K. Lim, S. P. Choi, and C. W. Chung, "Inductively coupled plasma reactive ion etching of titanium nitride thin films in a Cl_2/Ar plasma," *J. Ind. Eng. Chem.*, vol. 14, no. 3, pp. 297–302, May 2008.

[41] R. Hellriegel, M. Albert, B. Hintze, H. Winzig, and J. W. Bartha, "Remote plasma etching of titanium nitride using NF_3/argon and chlorine mixtures for chamber clean applications," *Microelectron. Eng.*, vol. 84, no. 1, pp. 37–41, Jan. 2007.

[42] A. K. Sinha and T. E. Smith, "Electrical properties of Si-N films deposited on silicon from reactive plasma," *J. Appl. Phys.*, vol. 49, no. 5, pp. 2756–2760, Aug. 2008.

[43] J. Song, J. Woo, S. Lee, A. Prakash, J. Yoo, K. Moon, and H. Hwang, "Steep slope field-effect transistors with Ag/TiO_2-based threshold switching device," *IEEE Electron Device Lett.*, vol. 37, no. 7, pp. 932–934, Jul. 2016.

[44] B.-G. Chae, J.-B. Seol, J.-H. Song, K. Baek, S.-H. Oh, H. Hwang, and C.-G. Park, "Nanometer-scale phase transformation determines threshold and memory switching mechanism," *Adv. Mater.*, vol. 29, no. 30, Jun. 2017, Art. no. 1701752.

[45] J. Song, J. Woo, A. Prakash, D. Lee, and H. Hwang, "Threshold selector with high selectivity and steep slope for cross-point memory array," *IEEE Electron Device Lett.*, vol. 36, no. 7, pp. 681–683, Jul. 2015.

[46] J. Yoo, J. Woo, J. Song, and H. Hwang, "Threshold switching behavior of Ag-Si based selector device and hydrogen doping effect on its characteristics," *AIP Adv.*, vol. 5, no. 12, Dec. 2015, Art. no. 127221.

[47] J.-H. Cha, S. Y. Yang, J. Oh, S. Choi, S. Park, B. C. Jang, W. Ahn, and S.-Y. Choi, "Conductive-bridging random-access memories for emerging neuromorphic computing," *Nanoscale*, vol. 12, pp. 14339–14368, Apr. 2020.

[48] S. Hwang, J.-J. Lee, M.-W. Kwon, M.-H. Back, T. Jang, J. Chang, J.-H. Lee, and B.-G. Park, "Analog complementary metal–oxide–semiconductor integrate-and-fire neuron circuit for overflow retaining in hardware spiking neural networks," *J. Nanosci. Nanotechnol.*, vol. 20, no. 5, pp. 3117–3122, May 2020.

[49] R. Aluguri and T.-Y. Tseng, "Overview of selector devices for 3-D stackable cross point RRAM arrays," *IEEE J. Electron Devices Soc.*, vol. 4, no. 5, pp. 294–306, Sep. 2016.

[50] M.-C. Wu, Y.-W. Lin, W.-Y. Jang, C.-H. Lin, and T.-Y. Tseng, "Low-power and highly reliable multilevel operation in ZrO_2 1T1R RRAM," *IEEE Electron Device Lett.*, vol. 32, no. 8, pp. 1026–1028, Jun. 2011.

[51] Y.-T. Su, H.-W. Liu, P.-H. Chen, T.-C. Chang, T.-M. Tsai, T.-J. Chu, C.-H. Pan, C.-H. Wu, C.-C. Yang, M.-C. Wang, S. Zhang, H. Wang, and S. M. Sze, "A method to reduce forming voltage without degrading device performance in hafnium oxide-based 1T1R resistive random access memory," *IEEE J. Electron Devices Soc.*, vol. 6, pp. 341–345, Feb. 2018.

[52] J.-W. Jang, S. Park, G. W. Burr, H. Hwang, and Y.-H. Jeong, "Optimization of conductance change in $Pr_{1-x}Ca_xMnO_3$-based synaptic devices for neuromorphic systems," *IEEE Electron Device Lett.*, vol. 36, no. 5, pp. 457–459, Apr. 2015.

[53] S. Kim, J. Chen, Y.-C. Chen, M.-H. Kim, H. Kim, M.-W. Kwon, S. Hwang, M. Ismail, Y. Li, X.-S. Miao, Y.-F. Chang, and B.-G. Park, "Neuronal dynamics in HfO_x/AlO_y-based homeothermic synaptic memristors with low-power and homogeneous resistive switching," *Nanoscale*, vol. 11, no. 1, pp. 237–245, Nov. 2018.

[54] J. Woo, K. Moon, J. Song, M. Kwak, J. Park, and H. Hwang, "Optimized programming scheme enabling linear potentiation in filamentary HfO_2 RRAM synapse for neuromorphic systems," *IEEE Trans. Electron Devices*, vol. 63, no. 12, pp. 5064–5067, Oct. 2016.

[55] M.-W. Kwon, M.-H. Baek, S. Hwang, S. Kim, and B.-G. Park, "Spiking neural networks with unsupervised learning based on STDP using resistive synaptic devices and analog CMOS neuron circuit," *J. Nanosci. Nanotechnol.*, vol. 18, no. 9, pp. 6588–6592, Sep. 2018.

[56] S. Hwang, H. Kim, J. Park, M.-W. Kwon, M.-H. Baek, J.-J. Lee, and B.-G. Park, "System-level simulation of hardware spiking neural network based on synaptic transistors and I&F neuron circuits," *IEEE Electron Device Lett.*, vol. 39, no. 9, pp. 1441–1444, Jul. 2018.

[57] H. Kim, S. Hwang, J. Park, S. Yun, J. H. Lee, and B. G. Park, "Spiking neural network using synaptic transistors and neuron circuits for pattern recognition with noisy images," *IEEE Electron Device Lett.*, vol. 39, no. 4, pp. 630–633, Feb. 2018.

[58] D. Lee, M. Kwak, K. Moon, W. Choi, J. Park, J. Yoo, J. Song, S. Lim, C. Sung, W. Banerjee, and H. Hwang, "Various threshold switching devices for integrate and fire neuron applications," *Adv. Electron. Mater.*, vol. 5, no. 9, Feb. 2019, Art. no. 1800866.

[59] M. Tao, D. Park, S. N. Mohammad, D. Li, A. E. Botchkerav, and H. Morkoç, "Electrical conduction in silicon nitrides deposited by plasma enhanced chemical vapour deposition," *Philos. Mag.*, vol. 73, no. 4, pp. 723–736, Sep. 2006.

[60] S. Fleischer, P. T. Lai, and Y. C. Cheng, "Simplified closed-form trap-assisted tunneling model applied to nitrided oxide dielectric capacitors," *J. Appl. Phys.*, vol. 72, no. 12, pp. 5711–5715, Jun. 1998.

[61] R. Perera, A. Ikeda, R. Hattori, and Y. Kuroki, "Trap assisted leakage current conduction in thin silicon oxynitride films grown by rapid thermal oxidation combined microwave excited plasma nitridation," *Microelectron. Eng.*, vol. 65, no. 4, pp. 357–370, May 2003.

[62] K. M. Kim, B. J. Choi, Y. C. Shin, S. Choi, and C. S. Hwang, "Anode-interface localized filamentary mechanism in resistive switching of TiO_2 thin films," *Appl. Phys. Lett.*, vol. 91, no. 1, Jul. 2007, Art. no. 012907.

[63] S.-K. Kim and Y.-S. Kim, "Charge carrier injection and transport in QLED layer with dynamic equilibrium of trapping/de-trapping carriers," *J. Appl. Phys.*, vol. 126, no. 3, Jul. 2019, Art. no. 035704.

[64] H. Sun, Q. Liu, C. Li, S. Long, H. Lv, C. Bi, Z. Huo, L. Li, and M. Liu, "Direct observation of conversion between threshold switching and memory switching induced by conductive filament morphology," *Adv. Funct. Mater.*, vol. 24, no. 36, pp. 5679–5686, Sep. 2014.

[65] S. Munjal and N. Khare, "Multilevel resistive and magnetization switching in $Cu/CoFe_2O_4/Pt$ device: Coexistence of ionic and metallic conducting filaments," *Appl. Phys. Lett.*, vol. 113, no. 24, Nov. 2018, Art. no. 243501.

[66] Y. Kim, H. Choi, H. S. Park, M. S. Kang, K.-Y. Shin, S.-S. Lee, and J. H. Park, "Reliable multistate data storage with low power consumption by selective oxidation of pyramid-structured resistive memory," *ACS Appl. Mater. Interfaces*, vol. 9, no. 44, pp. 38643–38650, 2017, doi: 10.1021/acsami.7b10188.

[67] A. Belmonte, J. Radhakrishnan, L. Goux, G. L. Donadio, P. Kumbhare, A. Redolfi, R. Delhougne, L. Nyns, W. Devulder, T. Witters, A. Covello, G. Vereecke, A. Franquet, V. Spampinato, S. Kundu, M. Mao, H. Hody, and G. S. Kar, "Co active electrode enhances CBRAM performance and scaling potential," in *IEDM Tech. Dig.*, San Francisco, CA, USA, Dec. 2019, pp. 35.8.1–35.8.4.

[68] K. J. Laidler and M. C. King, "Development of transition-state theory," *J. Phys. Chem.*, vol. 87, no. 15, pp. 2657–2664, Jul. 1983.

[69] S. Yu, X. Guan, and H.-S. P. Wong, "On the stochastic nature of resistive switching in metal oxide RRAM: Physical modeling, Monte Carlo simulation, and experimental characterization," in *IEDM Tech. Dig.*, Washington, DC, USA, Dec. 2011, pp. 17.3.1–17.3.4.

[70] J. Guy, G. Molas, P. Blaise, M. Bernard, A. Roule, G. Le Carval, V. Delaye, A. Toffoli, G. Ghibaudo, F. Clermidy, B. De Salvo, and L. Perniola, "Investigation of forming, SET, and data retention of conductive-bridge random-access memory for stack optimization," *IEEE Trans. Electron Devices*, vol. 62, no. 11, pp. 3482–3489, Nov. 2015.

[71] S. Aldana, P. Garcia-Fernández, A. Rodríguez-Fernández, R. Romero-Zaliz, M. B. González, F. Jiménez-Molinos, F. Campabadal, F. Gómez-Campos, and J. B. Roldán, "A 3D kinetic Monte Carlo simulation study of resistive switching processes in $Ni/HfO_2/Si\text{-}n^+$-based RRAMs," *J. Phys. D, Appl. Phys.*, vol. 50, no. 33, Jul. 2017, Art. no. 335103.

[72] F. Pan, S. Yin, and V. Subramanian, "A detailed study of the forming stage of an electrochemical resistive switching memory by KMC simulation," *IEEE Electron Device Lett.*, vol. 32, no. 7, pp. 949–951, Jul. 2011.

[73] K. V. Chau and J. J. Gaffney, "A finite-difference model for heat and mass transfer in products with internal heat generation and transpiration," *J. Food Sci.*, vol. 55, no. 2, pp. 484–487, Mar. 1990.

[74] P. Zhuang and F. Liu, "Implicit difference approximation for the time fractional diffusion equation," *J. Appl. Math. Comput.*, vol. 22, no. 3, pp. 87–99, Oct. 2006.

[75] Y. Shi, X. Wang, and T.-P. Ma, "Electrical properties of high-quality ultrathin nitride/oxide stack dielectrics," *IEEE Trans. Electron Devices*, vol. 46, no. 2, pp. 362–368, Feb. 1999.

[76] Y. C. Yeo, Q. Lu, W. C. Lee, T.-J. King, C. Hu, X. Wang, X. Guo, and T. P. Ma, "Direct tunneling gate leakage current in transistors with ultrathin silicon nitride gate dielectric," *IEEE Electron Device Lett.*, vol. 21, no. 11, pp. 540–542, Nov. 2000.

YEON-JOON CHOI (Graduate Student Member, IEEE) was born in Ulsan, South Korea, in 1993. He received the B.S. degree in electrical engineering from Seoul National University (SNU), South Korea, in 2017, where he is currently pursuing the Ph.D. degree in electrical engineering. His research interests include resistive switching random access memory and its application to synaptic device.

MIN-HWI KIM received the B.S. and Ph.D. degrees in electrical engineering from Seoul National University (SNU), in 2013 and 2020, respectively. In 2020, he joined Samsung Electronics Company Ltd., as a Staff Engineer in Flash Design Team of Memory Business Division.

SUHYUN BANG (Graduate Student Member, IEEE) received the B.S. degree from KAIST, Daejeon, South Korea, in 2015. He is currently pursuing the M.S. degree in electrical engineering with Seoul National University (SNU), Seoul, South Korea.

TAE-HYEON KIM (Graduate Student Member, IEEE) was born in Daejeon, South Korea, in 1992. He received the B.S. degree in electrical and computer engineering from Seoul National University (SNU), in 2015, where he is currently pursuing the Ph.D. degree in electrical and computer engineering. His research interests include resistive switching memory and neuromorphic systems.

DONG KEUN LEE (Member, IEEE) received the B.S. degree in electronic engineering from The Hong Kong University of Science and Technology, Hong Kong, in 2014, and the M.S. degree in electronic engineering from Seoul National University, in 2017, where he is currently pursuing the Ph.D. degree. His research interests include resistive switching random access memory and its application as a synaptic device.

KYUNGHO HONG (Member, IEEE) was born in Daejeon, South Korea, in 1992. He received the B.S. degree in electrical engineering from Seoul National University (SNU), Seoul, South Korea, in 2018, where he is currently pursuing the Ph.D. degree in electrical engineering.

CHAE SOO KIM received the B.S. degree in electrical engineering from Ewha Womans University, in 2018, and the M.S. degree in electrical engineering from Seoul National University (SNU), South Korea, in 2020. She is currently working with Samsung Electronics Company Ltd., DRAM PA Team of Memory Division.

SUNGJUN KIM (Member, IEEE) received the Ph.D. degree in electrical engineering from Seoul National University, Seoul, South Korea, in 2017 From 2017 to 2018, he was a Senior Engineer with Samsung Electronics Company Ltd., South Korea. In 2018, he joined Chungbuk National University, South Korea, as an Assistant Professor. In 2020, he also joined Dongguk University, Seoul, as an Assistant Professor.

SEONGJAE CHO (Senior Member, IEEE) received the B.S. and Ph.D. degrees in electronic engineering from Seoul National University, Seoul, South Korea, in 2004 and 2010, respectively. He worked as an Exchange Researcher with the National Institute of Advanced Industrial Science and Technology (AIST), Tsukuba, Japan, in 2009. Also, he worked as a Postdoctoral Researcher with Seoul National University in 2010 and Stanford University, Stanford, CA, USA, from 2010 to 2013. He is currently working as an Associate Professor with the Department of Electronic Engineering, Gachon University, South Korea. His research interests include emerging memory technologies, nanoscale CMOS devices, group-IV photonic devices, and hardware-driven neuromorphic devices and systems.

BYUNG-GOOK PARK (Fellow, IEEE) received the B.S. and M.S. degrees in electronics engineering from Seoul National University (SNU), in 1982 and 1984, respectively, and the Ph.D. degree in electrical engineering from Stanford University, in 1990. From 1990 to 1993, he worked with the AT&T Bell Laboratories, where he contributed to the development of 0.1 micron CMOS and its characterization. From 1993 to 1994, he was with Texas Instruments, developing 0.25 micron CMOS. In 1994, he joined SNU as an Assistant Professor at the School of Electrical Engineering (SoEE), where he is currently a Professor. In 2002, he worked with Stanford University as a Visiting Professor, on his sabbatical leave from SNU. He led the Inter-University Semiconductor Research Center (ISRC), SNU, as the Director from 2008 to 2010. His current research interests include the design and fabrication of nanoscale CMOS, flash memories, silicon quantum devices, and organic thin-film transistors. He has authored and coauthored over 1000 research articles in journals and conferences. He has served as a committee member for several international conferences, including Microprocesses and Nanotechnology, IEEE International Electron Devices Meeting, International Conference on Solid State Devices and Materials, and IEEE Silicon Nanoelectronics Workshop. He received Best Teacher Award from SoEE in 1997, Doyeon Award for Creative Research from ISRC in 2003, Haedong Paper Award from the Institute of Electronic Engineers of Korea (IEEK) in 2005, Educational Award from College of Engineering, SNU, in 2006, Haedong Research Award from IEEK in 2008, Nano Research Innovation Award from the Ministry of Science, ICT and Future Planning of Korea in 2013, and Research Excellence Award from Seoul National University in 2015. He has also served as an Editor for IEEE ELECTRON DEVICE LETTERS.